LOAD COMPENSATION AND VOLTAGE REGULATION IN THREE-PHASE FOUR-WIRE DISTRIBUTION SYSTEM USING PHOTOVOLTAIC SUPPORTED CUSTOM POWER DEVICE

Dr. C.K. Sundarabalan,
Assistant Professor
EEE Department
P.R.Engineering College
Thanjavur, Tamilnadu, India
ckseee@yahoo.com

Dr. K. Selvi
Associate Professor
EEE Department
Thiagarajar College of Engineering
Madurai, Tamilnadu,India
kseee@tce.edu

Abstract: *The necessity of good quality power is the obligatory one for today's power system due to the rapid growth of a nonlinear load, unbalanced load and sensitive load utilization in three-phase four-wire distribution system. In this paper, the photovoltaic (PV) supported Distribution Static Compensator (DSTATCOM) is used to mitigate unbalanced source current, current harmonics and neutral current. In addition, the thyristor-based solid state transfer switch (SSTS) is used in the proposed system to provide voltage regulation by transferring from the preferred source to the alternate source in case of a fault in the preferred source. Synchronous reference frame (SRF) theory is used to extract the reference current signals for the proposed DSTATCOM. The performance investigation of Adaptive Neuro Fuzzy Inference System (ANFIS) based DC voltage regulation is compared with the Proportional Integral (PI) controller under nonlinear and unbalanced linear load conditions. The effective voltage sag/swell detection is proposed to extract the transfer signal for SSTS. This paper shows that, the SSTS along with PV supported four-leg voltage source converter (VSC) based DSTATCOM topology simultaneously compensate both the current and voltage disturbances in three-phase four-wire distribution system. The effectiveness of the proposed system is analyzed in Matlab/Simulink.*

Key words: *ANFIS controller, PI controller, DSTATCOM, power quality, Voltage Sag*

1. Introduction

In present day electric power distribution systems, the quality of power is highly distorted due to extensive application of power electronic devices and other distorted loads [1]. In recent years, there has been a growing interest in custom power device (CPD) for power quality enhancement in distribution system. There are several types of CPD but the DSTATCOM and SSTS are considered in this work. DSTATCOM is a shunt connected compensating type CPD and its capable of mitigating current harmonics, load balancing, voltage regulation, neutral current compensation etc [2,3]. SSTS is one of a network reconfiguring type CPD and it is able to protect the load from voltage disturbances by transferring from the preferred feeder to the alternate feeder [4]. UPQC is another compensating type CPD, which is the combination of shunt and series active filter with a common DC capacitor and it is able to compensate both voltage and current related problems simultaneously [5]. Four-leg VSC based DSTATCOM eliminate the excessive neutral current without the help of a transformer [6]. In addition, this four-leg topology is most suitable for compensation of high neutral currents [7,8].

It has been observed from literature survey, the dynamic performance of the CPD is mainly dependent on its control strategy. It is renowned that the several investigations have been carried out for deriving the reference current signals for the DSTATCOM. The instantaneous reactive power theory (p–q theory) [9], SRF theory [10], Icos Φ theory [11], sliding mode control [12] etc. have been proposed to control the DSTATCOM. Due to lower computation, the SRF theory is used in this work for deriving the reference current signals.

Artificial Intelligence has been realized as a suitable tool for the analysis of power quality disturbances [13,14]. A DC voltage regulator is used to maintain the DC-link voltage of DSTATCOM at constant and equal to the specified reference value. Artificial intelligence based DC-link voltage controller gives better performance than PI controller [15]. The ANFIS combines both the learning abilities of a neural network and reasoning abilities of fuzzy logic [16]. In this work, the ANFIS based DC voltage regulation is proposed. Renewable energy placed a significant role in power quality improvement. As a matter of fact, the PV generation is considered as an important source in present day electric power system [17,18]. Recently researchers have focused on the distributed generation (DG) supported CPD for power quality improvement in distribution system [11,15,19].

In this paper, the PV supported four-leg DSTATCOM along with SSTS is modelled to mitigate current and voltage related power quality problems in three-phase four-wire distribution system. The PV array or battery is used to maintain the DC-link voltage of the four-leg DSTATCOM. The proposed system compensates neutral current, harmonic current, voltage sag, voltage swell and load balancing. Further, the performance of ANFIS based DC-link voltage regulation is investigated with the performance of PI controller under nonlinear and unbalanced linear load conditions. Matlab/Simulink results are provided to validate the dynamic performance of the proposed system.

2. Configuration

The Table 1 shows the difference between the proposed topology with the existing SRF based DSTATCOM topology. Several work in this area mainly focused on load compensation alone. In [2] and [20] both voltage regulation and load balancing are done but simultaneous compensation is not fulfilled. The proposed work focuses on the simultaneous compensation in distribution system using SSTS with DSTATCOM.

Table 1 Comparison of Existing SRF based DSTATCOM topology with the proposed system.

DSTATCOM Topology	Existing topology					Proposed system
	[2]	[19]	[20]	[21]	[22]	
Load balancing	✓	✓	✓	✓	✓	✓
Voltage regulation	✓	–	✓	–	–	✓
DG supported DSTATCOM	–	✓	–	–	–	✓
Four-leg VSC	✓	–	–	–	–	✓
ANFIS controller	–	–	–	–	–	✓
SSTS	–	–	–	–	–	✓

The detailed configuration of the proposed three-phase four-wire system is shown in Fig. 1. The power supply to the nonlinear or unbalanced load is supplied by the two sources namely preferred source and alternate source. During normal operations, the preferred source supplies power to the load through the preferred feeder. When a voltage disturbance occurs in the preferred feeder or preferred source, the SSTS quickly transfers the supply to the alternate feeder. In order to eliminate reactive current and harmonic current in the source side the proposed shunt connected DSTATCOM injects the appropriate converter current. Further, the fourth leg of the DSTATCOM provides neutral current elimination in the source side. The PV array or battery is used to maintain the DC capacitor voltage through the DC-DC boost converter. The ripple filter is connected in shunt with the load terminals to eliminate switching harmonics produced by the VSC. All the parameters used in the planned system are given in the Appendix.

3. Photovoltaic

The PV systems are renowned as a significant alternative among the renewable energy sources that will secure the availability of energy in future [17, 23]. The PV array composed of several PV modules

$$I_{PV} = N_P I_{ph} - N_p I_o \left[e^{\left(\frac{q\left(V_{PV}/N_s + I_{PV}R_{se}/N_p\right)}{KT_cA} \right)} - 1 \right] - \frac{\left(N_P V_{PV}/N_s + I_{PV}R_{se}\right)}{R_{sh}} \quad (1)$$

Where, I_{PV} is the PV module current (A), V_{PV} is the terminal voltage (V), I_{ph} is the light generated current in a PV module (A), I_O is the PV panel reverse saturation current (A), K is Boltzmann constant ($1.38\times10{-}23$ J/K), T_C is the junction temperature (K), q is the electron charge ($1.609 \times 10{-}19$ C), N_P is the number of cells in parallel, N_S is the number of cells in series, R_{se} is the series resistance (Ω) and R_{sh} is the parallel resistance (Ω). The SOLKAR-36 W PV module proposed in this work has been developed based on the model presented and validated in [24]. The determination of R_{se} and R_{sh} is carried out using [25]. The table 2 summarizes the parameters of the PV module.

Table 2 Electrical parameters of the PV module.

Parameter	Value
V_{oc}	21 V
I_{sc}	2.5 A
V_{mpp}	16.56 V
I_{mpp}	2.25 A
R_{se}	0.455 Ω
R_{sh}	174.4156 Ω
Ideality factor	1.6
No. of cells in series	36
No. of cells in parallel	1

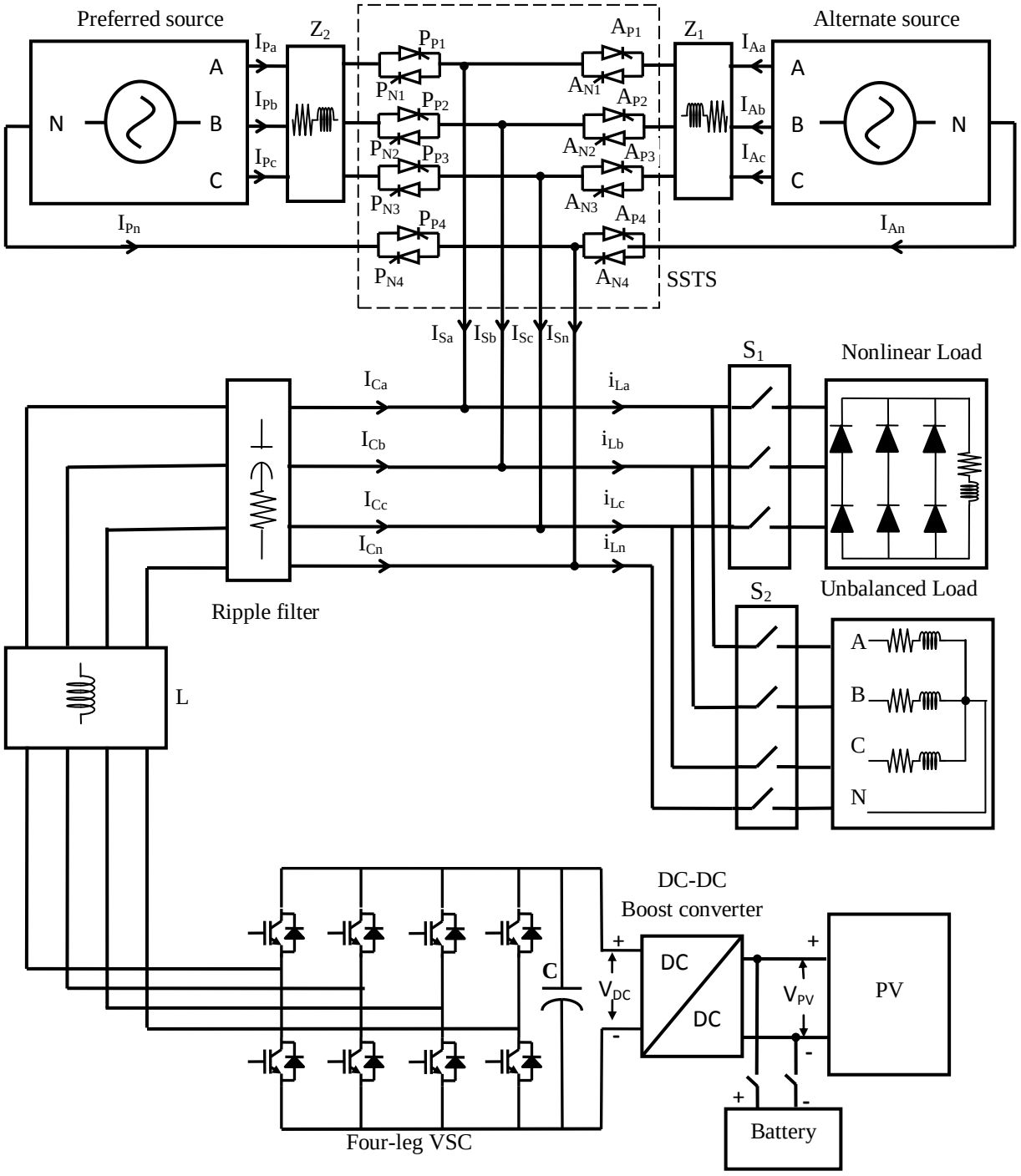

Fig. 1. Schematics of proposed methodology.

The required input voltage of the DC-DC converter can be obtained from (1-0.55) ×700=315 V. Where 0.55 and 700 are the duty ratio and output voltage of the DC-DC converter respectively. The design of DC-DC converter is carried out using [26]. The rated operating point of the proposed PV module is 2.25 A and 16.56 V. The number of PV modules required is calculated by using Eqs. (2) and (3).

$$PV_{series} = \frac{V_{PV}}{V_{PV1}} = \frac{315}{16.56} \cong 19 \quad (2)$$

$$PV_{parallel} = \frac{P_{PV}}{PV_{series} \times 0.36\,kW} = \frac{6\,kW}{19 \times 0.36\,kW} \cong 9 \quad (3)$$

The effect of irradiance and temperature on the current-voltage (*I-V*) characteristics of PV module is shown in Fig. 3. It is observed that, the higher irradiance with lower temperature generates maximum PV power.

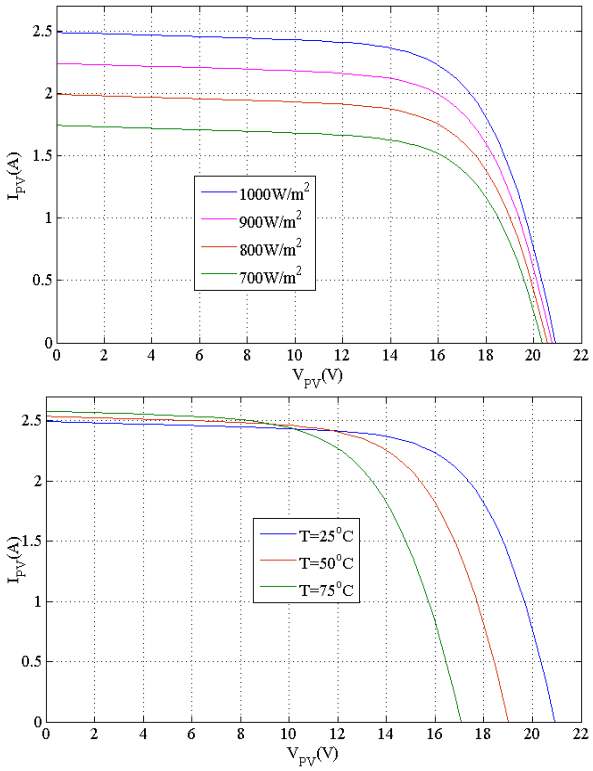

Fig. 3. Effect of irradiance and temperature on the I-V characteristics of PV module.

The proposed PV array composed of (19×9) modules with the power rating of 6 kW. The DC-DC converter is used to boost up the incoming PV voltage from 315 V to 700 V DC. The Battery is used to support the DSTATCOM during night-time and lower irradiation condition.

4. SSTS

The SSTS can be used very effectively to protect sensitive loads against voltage sag, swell and other electrical disturbances [1,27,28]. The SSTS is the combination of two thyristor block [4]. Each block composed of four thyristor modules corresponding to the three-phase four-wire system. Each thyristor module composed of two sets of thyristor switches connected in opposed directions. Preferred feeder voltage is continuously monitored by the proposed control logic. When the preferred source has an appropriate voltage, control logic turns on thyristors on the preferred feeder side. If any voltage sag or swell is detected from the preferred side voltage then alternate feeder transfer is initiated by removing gating pulses from the thyristors on the preferred feeder switch and firing thyristors on the alternate feeder side.

4.1. Voltage Disturbances Detection Logic

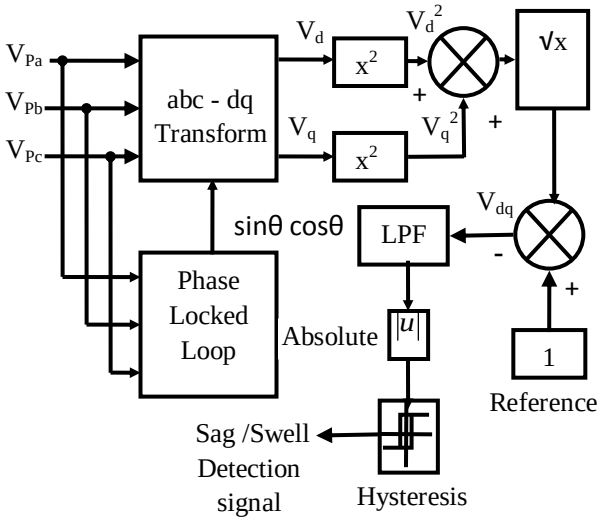

Fig. 4. Block diagram of proposed voltage sag/swell detection.

The block diagram of the proposed voltage sag/swell detection method is shown in Fig. 4. The three phase voltage (V_{pa}, V_{pb} and V_{pc}) from preferred source are transformed into (V_d and V_q).

$$V_d = \frac{2}{3}\left[V_{Pa}\sin(\omega t) + V_{Pb}\sin(\omega t - 2\pi/3) + V_{Pc}\sin(\omega t + 2\pi/3)\right] \quad (4)$$

$$V_q = \frac{2}{3}\left[V_{Pa}\cos(\omega t) + V_{Pb}\cos(\omega t - 2\pi/3) + V_{Pc}\cos(\omega t + 2\pi/3)\right] \quad (5)$$

$$V_{dq} = \sqrt{V_d^2 + V_q^2} \quad (6)$$

The obtained V_{dq} signal from Eq. (6) is compared with the reference value (1 pu) and filtered using LPF. The absolute value of the resulting variable is subjected to a hysteresis comparator and the output of this comparator generates the sag/swell detection signal. This signal is 0 when a sag/swell occurs, otherwise it is 1.

5. DSTATCOM

The DSTATCOM composed of four-leg VSC connected in shunt with the DC capacitor [2]. When DSTATCOM connected in the load terminals, it will inject the converter current in order to eliminate harmonic contents, DC offset in load and cancels the effect of unbalanced loads in the distribution system. Moreover DSTATCOM can perform voltage regulation while it is connected to a distribution bus [1,29]. In this paper, the DSTATCOM is connected in shunt with load terminals, so it is capable of performing load compensation only. To overcome the above shortcoming, SSTS is used for voltage regulation. The performance of the DSTATCOM mainly depends on the control algorithms, switching scheme and design of circuit components [30].

5.1 DSTATCOM controller

The extraction of reference currents using PI controller based SRF theory is shown in Fig. 5. The load currents from a-b-c co-ordinates (I_{La}, I_{Lb}, I_{Lc}) are converted into d-q-0 co-ordinates (I_d, I_q, I_0).

$$I_d = \frac{2}{3}\left[I_{La}\sin(\omega t) + I_{Lb}\sin(\omega t - 2\pi/3) + I_{Lc}\sin(\omega t + 2\pi/3)\right] \quad (7)$$

$$I_q = \frac{2}{3}\left[I_{La}\cos(\omega t) + I_{Lb}\cos(\omega t - 2\pi/3) + I_{Lc}\cos(\omega t + 2\pi/3)\right] \quad (8)$$

$$I_0 = \frac{1}{3}\left[I_{La} + I_{Lb} + I_{Lc}\right] \quad (9)$$

Each current component has an average value of DC component referred as I_{d1} and an oscillating value or ac component as I_{d2}.

$$I_d = I_{d1} + I_{d2} \quad (10)$$

The output of PI controller at the DC bus voltage of DSTATCOM is considered as the current (i_{loss}) for meeting its losses.

$$I_{loss(n)} = I_{loss(n-1)} + K_{pd}(V_{de(n)} - V_{de(n-1)}) + K_{id}V_{de(n)} \quad (11)$$

Where $V_{de(n)}$ is the error between reference and sensed DC voltage at the nth sampling instant. K_{pd} and K_{id} are the proportional and integral gains. Therefore the reference source current is,

$$I_d^* = I_{d1} + I_{loss} \quad (12)$$

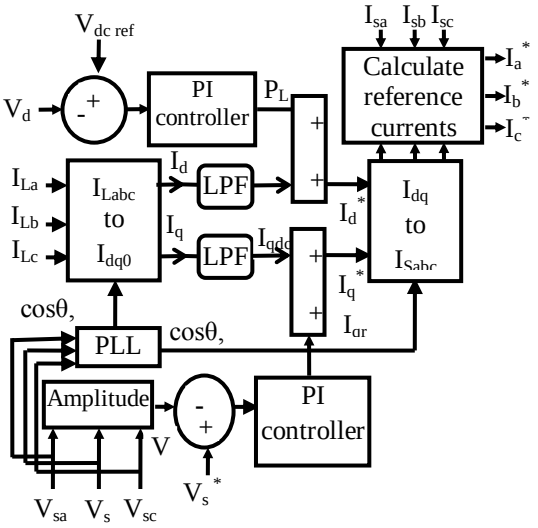

Fig. 5. Generation of reference current using PI controller based SRF theory.

Similarly in quadrature component, average value of DC component is referred as I_{q1} and oscillating quantity as I_{q2}.

$$I_q = I_{q1} + I_{q2} \quad (13)$$

$$I_{qr(n)} = I_{qr(n-1)} + K_{pq}(V_{te(n)} - V_{te(n-1)}) + K_{iq}V_{te(n)} \quad (14)$$

$$I_q^* = I_{q1} + I_{qr} \quad (15)$$

The reference source currents in the a–b–c frame are obtained by reverse transformation of the current vector.

$$I^*_a = I_d^* \sin\omega t + I_q \cos\omega t \quad (16)$$

$$I^*_b = I_d^* \sin(\omega t - 2\pi/3) + I_q \cos(\omega t - 2\pi/3) \quad (17)$$

$$I^*_c = I_d^* \sin(\omega t + 2\pi/3) + I_q \cos(\omega t + 2\pi/3) \quad (18)$$

The sensed source currents (I_{sa}, I_{sb}, I_{sc}) are compared with the generated reference source currents (I_a*, I_b*, I_c*) and the resulted current is fed to the hysteresis controller to generate gate pulses. The parameters of DC-link voltage PI controller are same as [15].

5.2. Generation of Neutral current reference signal.

The extraction of reference current signal for fourth-leg of VSC in DSTATCOM is obtained by using Eq. (19).

$$i_n^* = -\left(i_{La} + i_{Lb} + i_{Lc}\right) \tag{19}$$

The switching signals for the fourth-leg of VSC in DSTATCOM are generated from the error signal by comparing the load current and reference [2]. The extracted signal is fed to hysteresis controller to generate switching pulses for the fourth-leg of VSC in DSTATCOM.

5.3 ANFIS controller based DC voltage regulation in four-leg DSTATCOM

The ANFIS utilize the learning mechanism of neural network for determining the membership function parameters of the fuzzy logic [16,31].

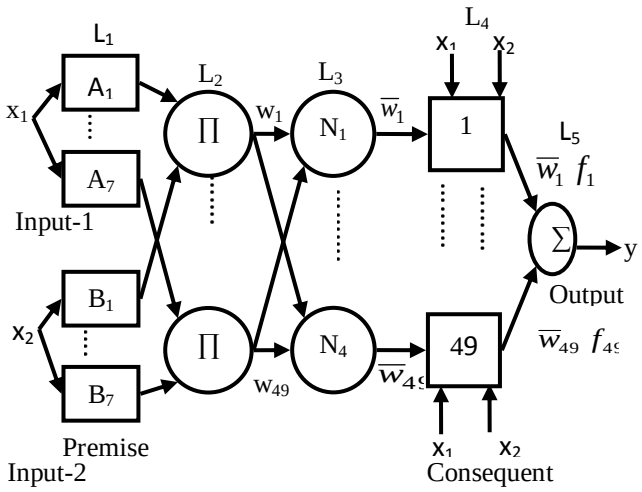

Fig. 6. ANFIS architecture.

The data collected from input and output of the PI controller are used to train the ANFIS controller. The first input (x_1) and the second input (x_2) is the error and change in error between the actual and reference DC voltage respectively. The proposed ANFIS controller has five layers, two inputs (x_1 and x_2) and one output(y) is shown in Fig. 6. The node functions of five layers displayed in the ANFIS architecture are enlightened as follows [16]. The node presented in layer-1 is symbolized by a square. Where x_1 is the input to the node i, and A_i is the linguistic label (*A1, A2, A3, A4, A5, A6* and *A7*) linked with this node function. The detailed procedure to generate ANFIS controller in Matlab is shown in Fig. 7.

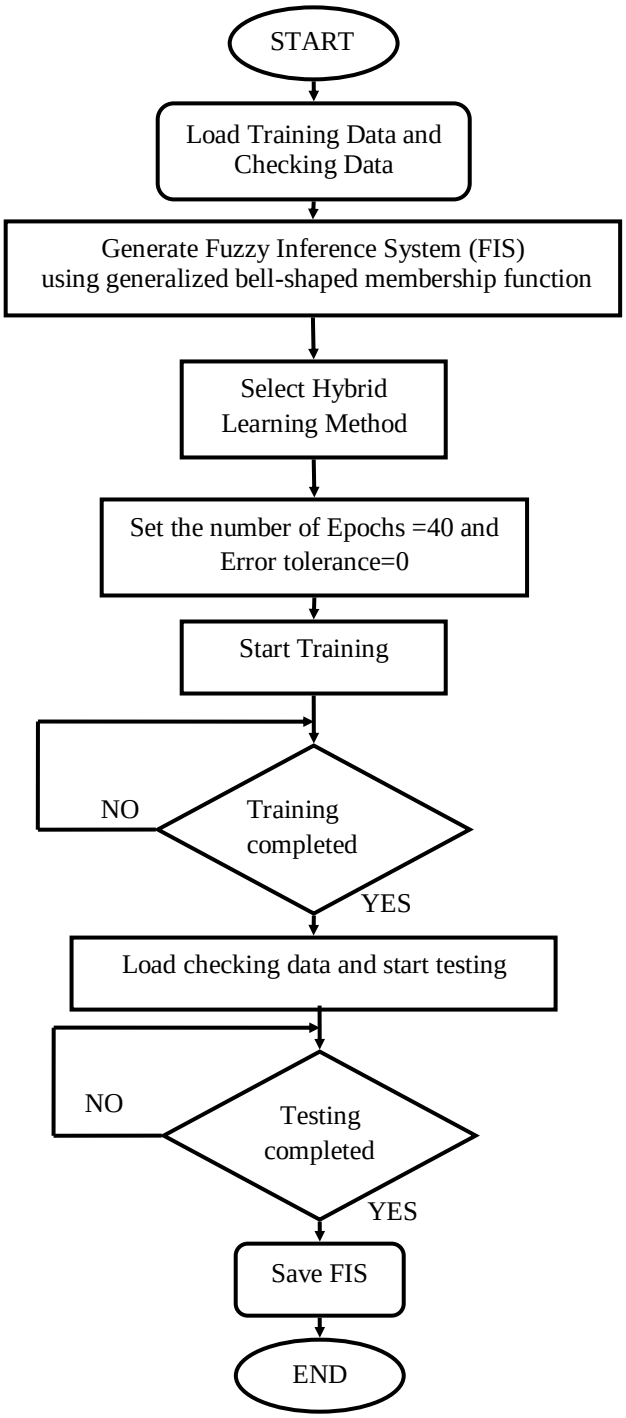

Fig. 7. Flowchart of ANFIS training and testing in Matlab.

In this work, seven generalized bell-shaped membership functions are used and the corresponding node equations are given below.

$$O_i^1 = \mu A_i(x_1) \tag{20}$$

The parameter in layer-1 is referred as premise parameters. The node presented in layer-2 is symbolized by a circle and labeled as $\prod$.

$$\mu A_i(x_1) = \frac{1}{1+\left|\frac{x_1 - c_i}{a_i}\right|^{2b_i}} \tag{21}$$

These layers multiply the incoming signals and forward it to the layer-3.

$$w_j = \mu A_i(x_1) \times \mu B_i(x_2) \tag{22}$$

The output from each node in layer-2 represents the firing strength of a rule. Each node presented in layer-3 is symbolized by a circle and labeled as N. The output of this layer calculates the normalized firing strength of every rule.

$$\overline{w}_j = \frac{w_j}{\sum_{k=1}^{49} w_k} \tag{23}$$

Each node presented in layer-4 is symbolized by a square. The parameter in layer-4 is referred as consequent parameters.

$$O_j^4 = \overline{w}_j \; f_j = \overline{w}_j \left(r_j x_1 + s_j x_2 + t_j\right) \tag{24}$$

Rule base

If $x_1$is $A_1$and $x_2$is B_1 then $f_1 = r_1 x_1 + s_1 x_2 + t_1$

If $x_1$is $A_1$and $x_2$is B_2 then $f_2 = r_2 x_1 + s_2 x_2 + t_2$

.

.

If $x_1$is A_7 and $x_2$is B_7 then $f_{49} = r_{49} x_1 + s_{49} x_2 + t_{49}$

Single node is presented in layer-5 which is symbolized by a circle and labeled as $\sum$. This layer calculates the output (y) by summing up of all incoming signals.

$$y = \sum_{j=1}^{49} \overline{w}_j \; f_j = \sum_{j=1}^{49} \left[\left(\overline{w}_j x_1\right) r_j + \left(\overline{w}_j x_2\right) s_j + \left(\overline{w}_j\right) t_j\right] \tag{25}$$

Where,

i =1, 2… 7 and j=1, 2… 49.

O_i^1 = output of the i_{th} node in layer1

a_i, b_i, c_i = Parameters of generalized bell-shaped membership function

O_j^4 = output of the i_{th} node in layer4

$\overline{w}_j$ = Layer-3 output

r_j, s_j, t_j = consequent parameter set which are determined during training

A_i, B_i = fuzzy membership function

The square node is an adaptive node and its parameters are changed during training but the parameters presented in circle nodes are fixed. The initial and final membership functions of Input-1 and Input-2 of ANFIS controller are shown in Fig. 8.

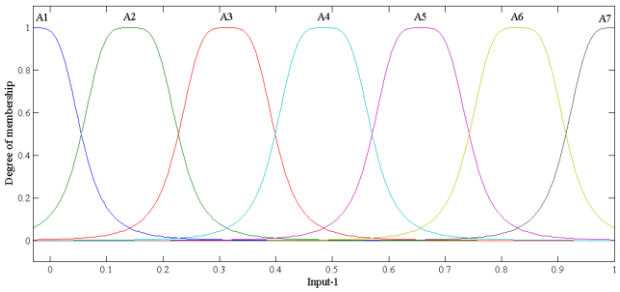

(a) Initial generalized bell-shaped membership function of input-1 (x_1).

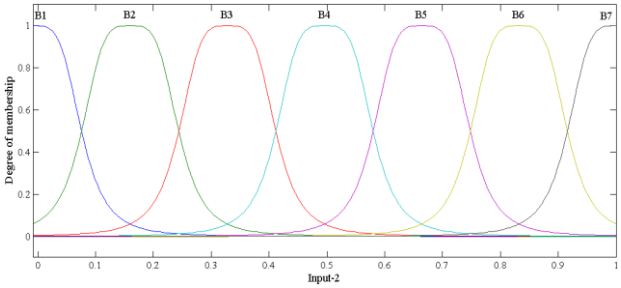

(b) Initial generalized bell-shaped membership function of input-2 (x_2).

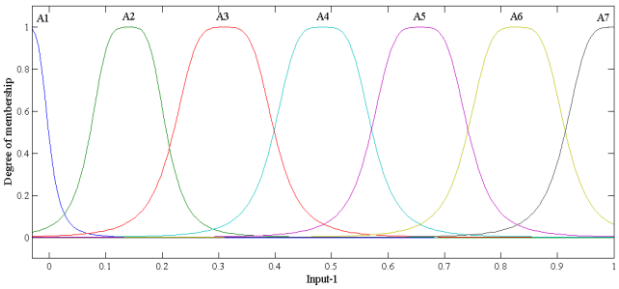

(c) Final generalized bell-shaped membership function of input-1(x_1).

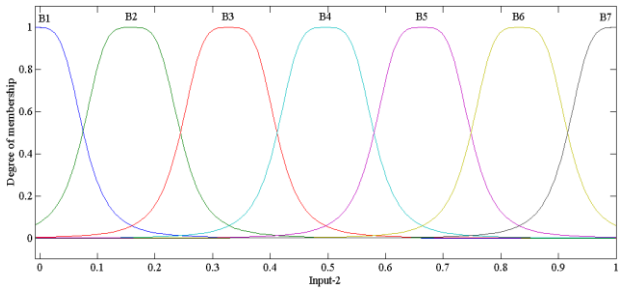

(d) Final generalized bell-shaped membership function of input-2 (x_2).

Fig. 8. Initial and final generalized bell-shaped membership function of input-1 and input-2.

The proposed ANFIS uses a hybrid learning algorithm which is the combination of the least-squares method and the backpropagation gradient descent method. In hybrid learning every iteration composed of the forward pass and backward pass. During forward pass, the premise parameters are fixed and the consequent parameters are adjusted by the least square method, while in backward pass, the error signals propagate backwards here the consequent parameters are fixed and the premise parameters are adjusted by the gradient descent method [16].

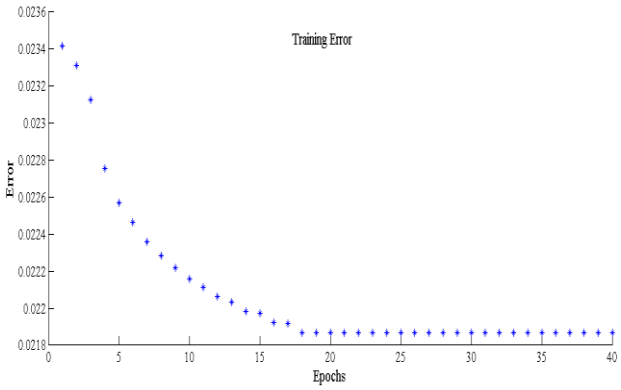

Fig. 9. Training error versus epochs plot.

The ANFIS used here contains 49 rules, with 7 generalized bell-shaped membership functions being assigned to each input variable. 25001 training data was used for training of ANFIS and 25000 checking data was used for verifying the identified ANFIS. Fig. 9 shows the training error values for each epoch. The three dimensional surface view of generated ANFIS controller is shown in Fig. 10. The detailed information about the proposed ANFIS controller is given in Table 3.

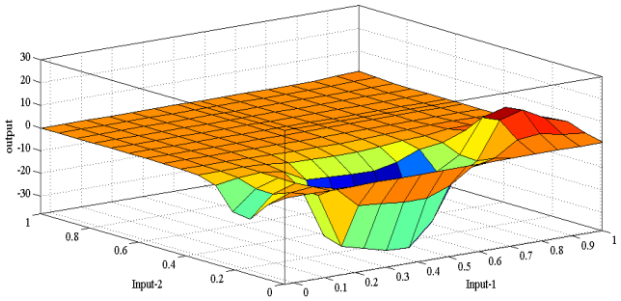

Fig. 10. Surface view of ANFIS controller.

Table 3 ANFIS Parameters used for Training.

Parameter of ANFIS	value
Number of Epoch	40
Number of nodes:	131
Number of linear parameters:	49
Number of nonlinear parameters:	42
Total number of parameters:	91
Number of training data pairs:	25001
Number of checking data pairs:	25000
Number of fuzzy rules:	49

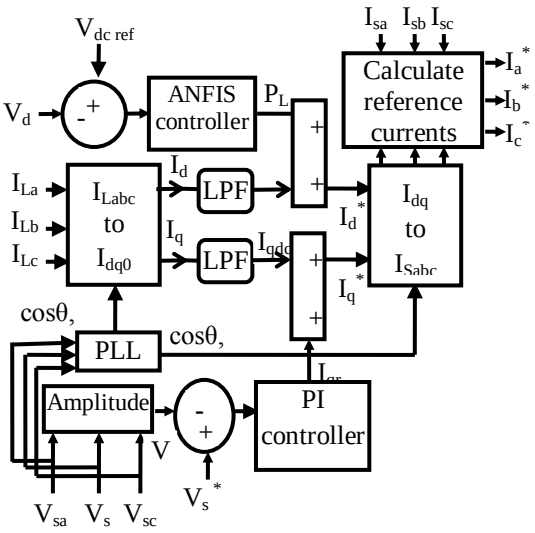

Fig. 11. Generation of reference current using ANFIS controller based SRF theory.

The extraction of reference current signals with ANFIS controller based SRF theory is shown in Fig. 11. The ANFIS controller controls the small amount of active current by comparing the actual DC-link voltage of DSTATCOM with the reference voltage and the output of this controller is the corresponding power flow needed to maintain the DC-link voltage. Hence this power flow is added as a part of reference for current controller which

controls the inverter to provide the required compensation current and maintain the DC-link voltage of the DSTATCOM.

6. Results and Discussions

The performance of the proposed SRF based DSTATCOM is analyzed with both nonlinear and unbalanced linear load under voltage sag and swell conditions.

6.1. Performance of the DSTATCOM with the nonlinear load condition

The load balancing, voltage regulation and current harmonic compensation performance of the DSTATCOM with SSTS under nonlinear load condition is shown from Fig. 12 to Fig. 17. The SSTS transfer signal for both preferred feeder and alternate feeder under voltage sag and swell condition is shown in Fig. 12. The nine subplots of Figs. 13 and 14 illustrate, preferred source voltages (V_P), alternate source voltages (V_A), point of common coupling voltages (V_S), preferred source currents(I_P), alternate source currents (I_A), load currents (I_L), converter currents (I_C), source currents (I_S) and DC-link voltage (V_{DC}) under nonlinear load condition.

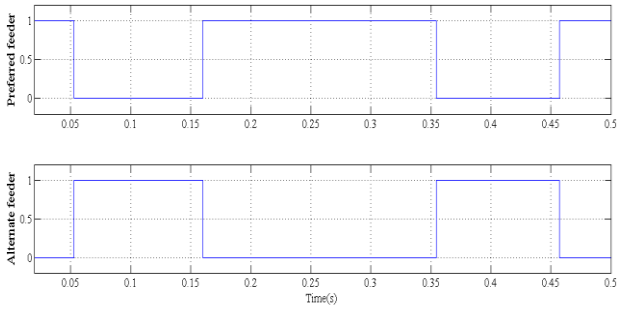

Fig. 12. SSTS transfer signal under voltage sag and swell conditions.

Figs.13 and 14 illustrate the performance of the PI and ANFIS based DSTATCOM with SSTS under nonlinear load with voltage sag and swell conditions. The three-phase to ground fault is applied in the preferred feeder from 0.05 s to 0.15 s. It is observed from Fig. 13 and 15, 65% three-phase voltage sag is occurred in the V_P. Due to effective control strategy of the SSTS, the preferred feeder switches are turned OFF and the alternate feeder switches turns ON at 0.052 s. So that, the point of common coupling voltages (V_S) is not affected by the voltage sag disturbance. After the completion of the voltage sag duration, the preferred feeder again connects to the load and the alternate feeder switches are turned OFF. The three-phase voltage swell is created in the preferred feeder from 0.35 s to 0.45 s. It is observed that 50% three-phase voltage swell is occurred in the V_P. Due to effective control strategy of the SSTS, the preferred feeder switches are turned OFF and the alternate feeder switches turns ON at 0.354 s. So that, the point of common coupling voltages (V_S) will not be affected by the voltage swell disturbance. After the completion of the voltage swell duration, the preferred feeder again connects to the load and the alternate feeder switches are turned OFF. However the proposed control strategy detects voltage sag very quickly than voltage swell.

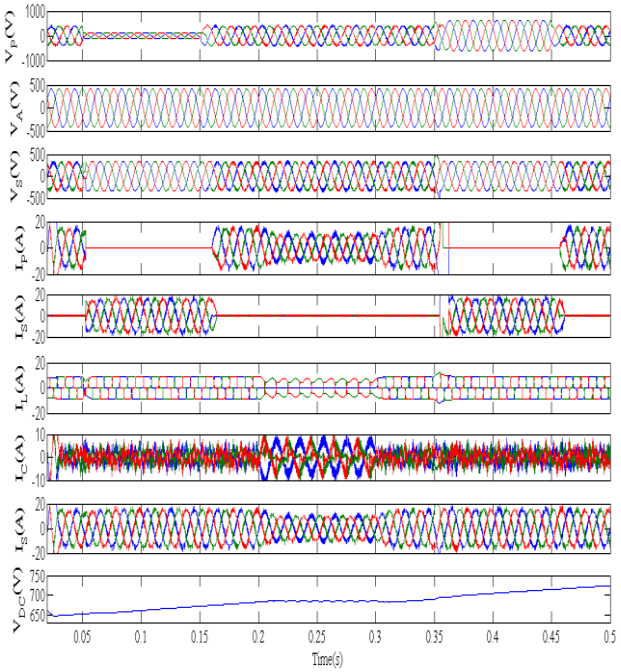

Fig. 13. Voltage regulation and load compensation with PI controller under nonlinear load with voltage sag and swell conditions.

It is observed from Figs. 13 and 14, due to the presence of nonlinear load in the distribution system, the load current (I_L) waveform is highly distorted. The PI controller and ANFIS controller based DSTATCOM compensate the harmonic current by injecting the required converter currents (I_C). So that, the source currents (I_S) are made sinusoidal, balanced and in-phase with the source voltage.

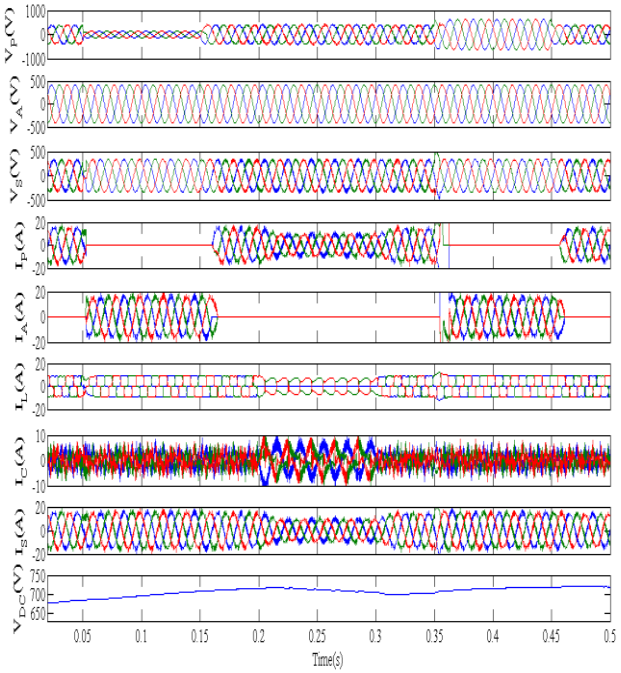

Fig. 14. Voltage regulation and load compensation with ANFIS controller under nonlinear load with voltage sag and swell conditions.

It is important to note that, the three-phase nonlinear load is changed to two-phase load from 0.2 s to 0.3 s. Due to the effective compensation of DSTATCOM the source currents are still sinusoidal and balanced even when the system is operated in two-phase load. Both the controllers have good performance in load balancing but the ANFIS controller has better DC voltage (V_{DC}) regulation than the PI controller under nonlinear load condition.

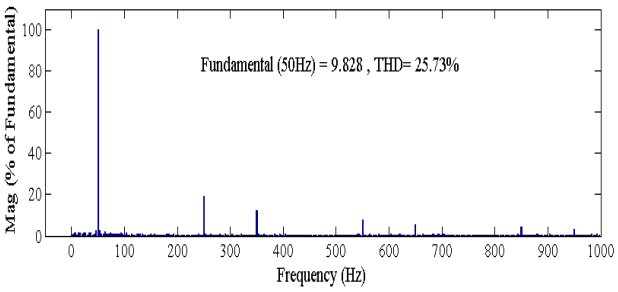

(a) Phase-a

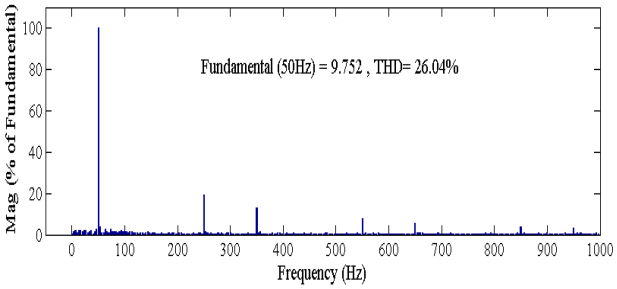

(b) Phase-b

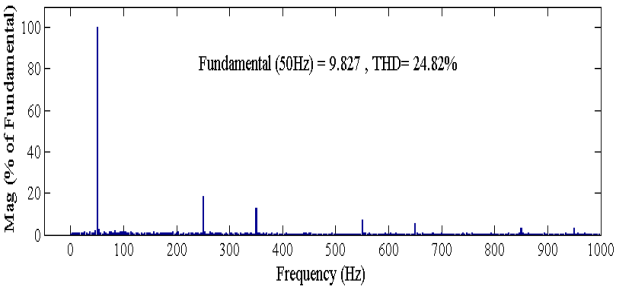

(c) Phase-c

Fig. 15. Harmonic spectrum of source current before compensation.

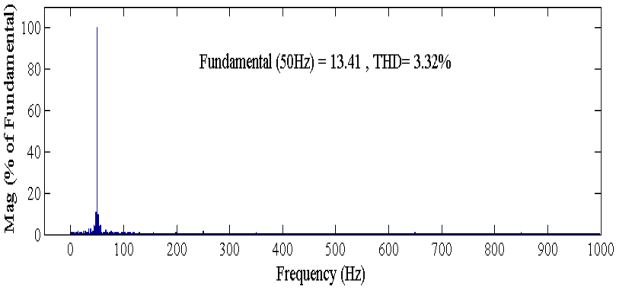

(a) Phase-a

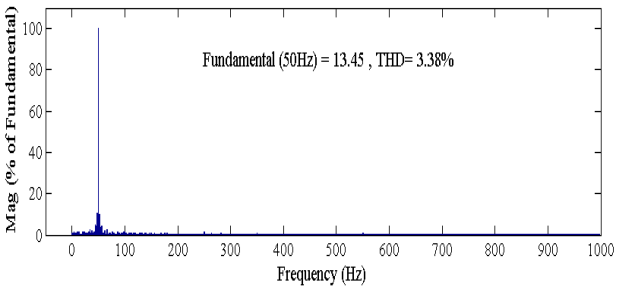

(b) Phase-b

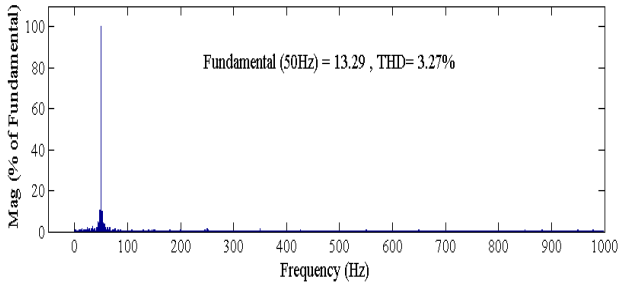

(c) Phase-c

Fig. 16. Harmonic spectrum of source current after compensation with PI controller.

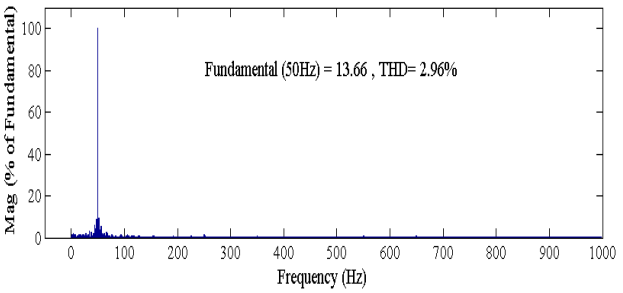

(a) Phase-a

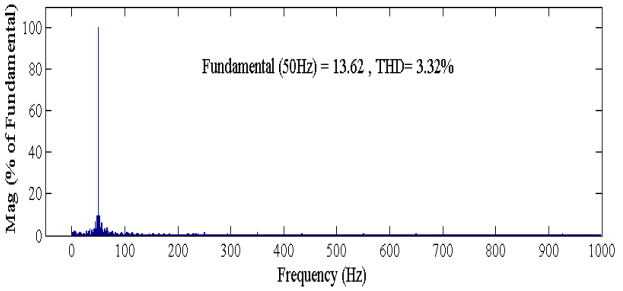

(b) Phase-b

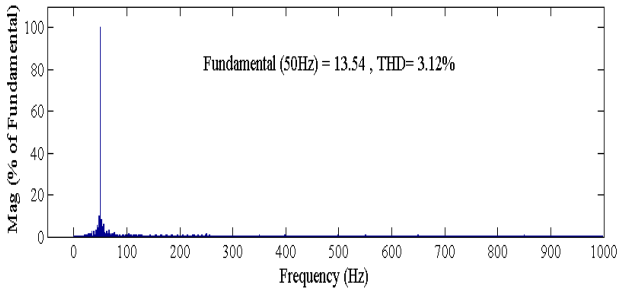

(c) Phase-c

Fig. 17. Harmonic spectrum of source current after compensation with ANFIS controller**.**

Fig. 15 illustrates the performance of total harmonic distortion (THD) before compensation in phase-a, phase-b and phase-c of source current are 25.73%, 26.04% and 24.82% respectively. It is observed from Fig. 16, after compensation with PI controller the THD of source current in phase-a, phase-b and phase-c are reduced to 3.32%, 3.38% and 3.27% respectively. In case of ANFIS controller the THD is reduced to 2.96%, 3.32% and 3.12% is shown in Fig. 17. It is noted that ANFIS controller has better harmonic compensation than PI controller.

Table 4 gives the comparison of the individual harmonic level of source current between the proposed PI controller and ANFIS controller. From this comparison, it is clearly shown that the harmonics presented in the source current are eliminated successfully. It is observed that the THD of I_s obtained from both PI controller and ANFIS controller fulfill the requirement of IEEE-519 standard. However the ANFIS controller offers better harmonic compensation than PI controller.

Table 4 Harmonic Contents of the source current.

H	Source current Harmonic Content (% of fundamental)								
	Before compensation			After compensation					
				PI controller			ANFIS controller		
	a	b	c	a	b	c	a	b	c
3	0.6	0.5	0.6	0.3	0.7	0.8	0.3	0.0	0.1
5	19.2	19.3	18.2	1.5	1.3	1.1	1.3	1.47	1.1
7	12.4	13.0	12.8	0.9	1.0	1.2	0.8	1.1	0.9
9	0.4	0.5	0.7	0.2	0.1	0.2	0.0	0.1	0.1
11	7.4	7.4	6.9	0.5	0.6	0.8	0.6	0.8	0.9
13	5.5	5.4	5.6	0.6	0.5	0.8	0.8	0.7	0.7
15	0.3	0.2	0.4	0.1	0.3	0.3	0.1	0.0	0.1
17	4.0	3.9	3.2	0.8	0.3	0.5	0.3	0.5	0.6
19	3.1	3.2	3.2	0.3	0.5	0.6	0.2	0.0	0.3
THD	25.7	26.0	24.8	3.3	3.3	3.2	2.9	3.3	3.1

H -Harmonic order

6.2. Performance of the DSTATCOM with the unbalanced linear load conditions

The performance of the DSTATCOM with SSTS under unbalanced linear load condition is shown from Fig. 18 to Fig. 20. The nine subplots of Fig. 18 and Fig. 19 illustrate, preferred source voltages (V_P), alternate source voltages (V_A), point of common coupling voltages (V_S), preferred currents (I_P), alternate currents (I_A), load currents (I_L), converter currents (I_C), source currents (I_S) and DC-link voltage (V_{DC}) under unbalanced linear load condition.

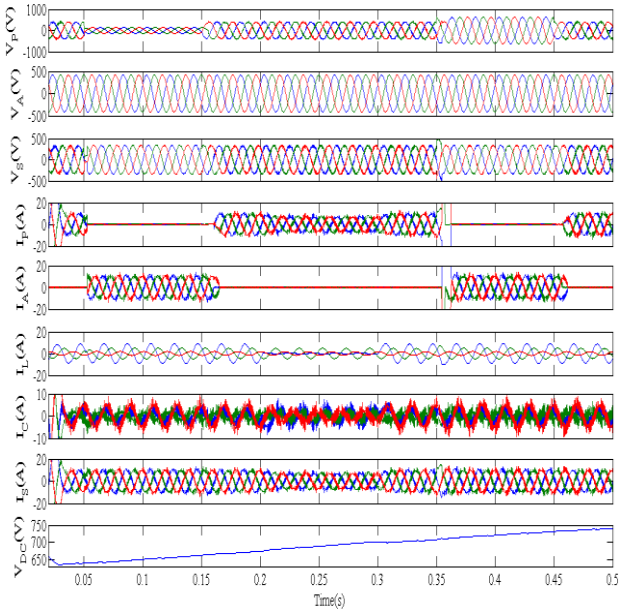

Fig. 18. Voltage regulation and load compensation with PI controller under unbalanced load with voltage sag and swell conditions.

A 65% three-phase voltage sag is applied in the preferred feeder at t=0.05 s and ends at t=0.15 s. The proposed SSTS control strategy detects the voltage sag, which turned off the preferred feeder thyristor and turns on the alternate feeder thyristors. It is observed from Figs. 18 and 19, during voltage sag, the alternate feeder gives full supply to the load. After the completion of voltage sag duration, the alternate feeder supply gets turned off and the preferred feeder gives supply to the load. A 50% three-phase voltage swell is applied in the preferred feeder at t=0.35 s and ends at t=0.4 s. The proposed SSTS control strategy detects the voltage swell, which turned off the preferred feeder thyristor and turns ON the alternate feeder thyristors. It is observed from Figs. 18 and 19, during voltage swell, the alternate feeder gives full supply to the load. After the completion of voltage swell duration, the alternate feeder supply gets turned off and the preferred feeder gives supply to the load.

Fig. 18 and Fig. 19 shows the performance of the PI and ANFIS based DSTATCOM for load balancing along with DC voltage regulation under unbalanced linear load with voltage sag and swell conditions. It is observed from the waveform of Figs. 18 and 19, the DSTATCOM injected the appropriate current for each phase to make the source currents sinusoidal balanced and in-phase with the source voltage. It is also observed that, from 0.2 s to 0.3 s, when the three-phase unbalanced linear load is changed to two-phase load the source currents (I_S) are still maintained sinusoidal and balanced. It is noteworthy that, both the controllers have good performance in load balancing but the ANFIS controller has better DC voltage regulation than the PI controller under unbalanced linear load condition.

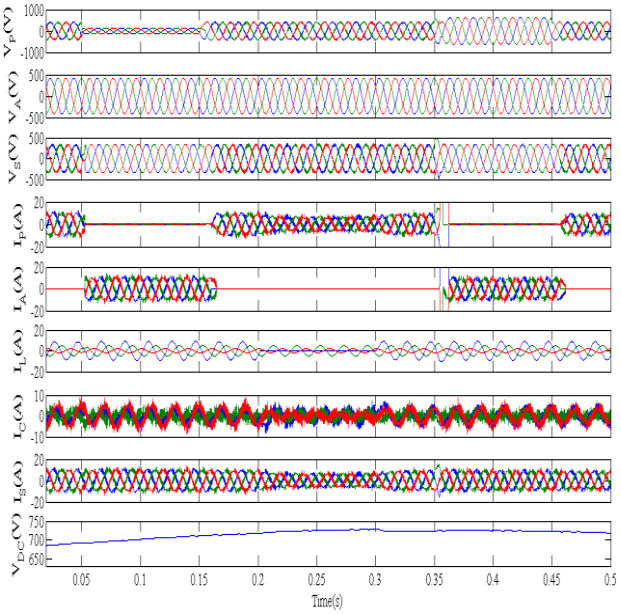

Fig. 19. Voltage regulation and load compensation with ANFIS controller under unbalanced load with voltage sag and swell conditions.

Neutral current will result in any circuit when there is unbalanced flow of current i.e when the load in the three-phases are not balanced there is a net flow of current through the neutral line. Here the system is provided with the unbalanced load and this leads to the flow of current through the neutral. The suitable control strategy is adopted to cancel the neutral current. In order to achieve zero neutral current at source side (I_{Sn}), the converter neutral current (I_{Cn}) is injected in opposite polarity with the load neutral current (I_{Ln}). It is observed from Fig. 20 the neutral current is fully eliminated and it is almost near to zero for both PI and ANFIS controller.

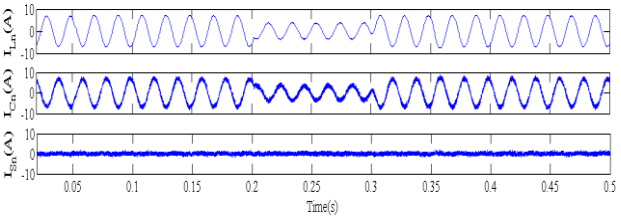

(a) PI controller

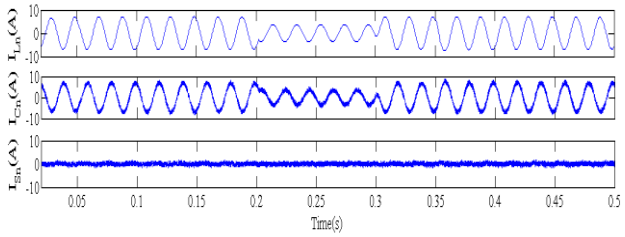

(b) ANFIS controller

Fig. 20. Source neutral current compensation.

6.3 Comparison of proposed work with existing work.

The Table 5 compares the THD compensation performance of various control algorithms such as symmetrical component (SC) theory, instantaneous reactive power (IRP) theory, instantaneous active and reactive current component (IARCC) theory and the proposed method. It is observed from this table the proposed ANFIS method offers better THD compensation than other methods.

Table 5 Comparison of %THD of source current with existing and proposed method.

I_s	Ph	Existing methods					Proposed Methods	
		IRP-PI [15]	IRP-ANFIS [15]	IRP [32]	SC [32]	IARCC [32]	SRF-PI	SRF ANFIS
THD %	a	3.06	3.08	2.83	3.98	3.79	3.32	2.96
	b	4.44	4.28	4.72	4.80	4.73	3.38	3.32
	c	4.08	3.92	4.65	4.29	4.60	3.27	3.12

7. Conclusion

The performance of three-phase four-wire DSTATCOM along with SSTS for the mitigation of power quality issues like voltage sag/swell, neutral current compensation, source harmonic reduction and load balancing are extensively simulated in MATLAB/ SIMULINK. In order to verify the performance of SSTS, the proposed system is analyzed with both voltage sag and swell conditions. It is clearly noticed that, the presented results have been confirmed the effectiveness of SSTS under both voltage disturbances. The SRF method has been presented for the extraction of reference current signals. The PV supported DSTATCOM injects current in such a way, to cancel out the excess neutral current, harmonic current and unbalanced source current. The load compensation along with voltage regulation is achieved by the combination of DSTATCOM with SSTS. Both ANFIS and PI controller based DSTATCOM compensates current harmonics successfully. Nevertheless the ANFIS based DC-link voltage regulation gives better performance than PI controller.

Acknowledgment

The authors gratefully acknowledge the management of P. R. Engineering College Thanjavur and Thiagarajar College of Engineering, Madurai, India, for providing all the facilities to do the research work.

Appendix

Source Voltage	3-phase, 4-wire, 415V,50 Hz
Line impedance	Rs = 0.01 Ω, Ls = 2.1 mH
DC-link voltage of DSTATCOM	700 V DC
DC-link capacitance of DSTATCOM	3000 µF
DC-link voltage PI controller	K_p=4.96 and K_i=1.01
Ripple filter	R_f=10 Ω, C_f=5 µF
Load:	R_1=30 Ω, L_1=70 mH, R_2=60 Ω, L_2=100 mH, R_3=120 Ω, L_3=400 mH.
Linear unbalanced load	3-phase uncontrolled bridge rectifier,
Nonlinear load	R_{DC} = 50 Ω, L_{DC} = 1 mH.

References

[1] A. Ghosh, G. Ledwich, Power quality enhancement using custom power devices, Kluwer 2002.

[2] B. Singh, P. Jayaprakash, D.P. Kothari, New control approach for capacitor supported DSTATCOM in three-phase four wire distribution system under non-ideal supply voltage conditions based on synchronous reference frame theory, Int. J. Electr Power Energy Syst. 33 (2011) 1109-1117.

[3] A. Shokri, H. Shareef, A. Mohamed, M. Farhoodnea, H. Zayandehroodi, A novel single-phase phase space-based voltage mode controller for distributed static compensator to improve voltage profile of distribution systems, Energy Convers. Manage. 79 (2014) 449–455.

[4] Seyedreza Aali, Unified Power Quality Conditioner Based on Neural-Network Controller for Mitigation of

Voltage and Current Source Harmonics, Journal of Electrical Engineering, pp 1-6.

[5] R. Yuanjie, C. Li, Q. Ding, An adaptive harmonic detection and a novel current control strategy for unified power quality conditioner, Simul. Modell. Pract. 17 (2009) 955-966.

[6] B. Singh, P. Jayaprakash, D.P. Kothari, A. Chandra, K.A. Haddad, Comprehensive study of DSTATCOM configurations, IEEE Trans. Ind. Inf. 10 (2014) 854-870.

[7] D. Sreenivasarao, P. Agarwal, B. Das, Neutral current compensation in three-phase, four-wire systems: A review, Electr. Power. Syst. Res. 86(2012) 170-180.

[8] Chebabhi, Ali, et al. "Three Level Four Leg Shunt Active Power Filter Based a New Three Dimensional Space Vector Modulation strategy in the αβ0-axes." Journal of Electrical Engineering, In Press, accepted 10.08 (2015).

[9] H. Akagi, E. Hirokazu Watanabe, M. Aredes, Instantaneous power theory and applications to power conditioning, Wiley-IEEE Press, 2007.

[10] G. Benysek, M. Pasko, Power Theories for Improved Power Quality, Springer, 2012.

[11] V. Kamatchi Kannan, N. Rengarajan, Investigating the performance of photovoltaic based DSTATCOM using I cosΦ algorithm, Int. J. Electr. Power Energy Syst. 54 (2014) 376–386.

[12] R. Gupta, A. Ghosh, Frequency-Domain Characterization of Sliding Mode Control of an Inverter Used in DSTATCOM Application, IEEE Trans. Circuits Syst. 53(2006) 662-676.

[13] W.R.A Ibrahim, M.M Morcos, Artificial Intelligence and Advanced Mathematical Tools for Power Quality Applications: A Survey, IEEE Trans. Power Delivery 17 (2002) 668-673.

[14] P. Kumar, A. Mahajan, Soft computing techniques for the control of an active power filter, IEEE Trans. Power Delivery 24 (2009) 452-461.

[15] C.K. Sundarabalan, K. Selvi, PEM fuel cell supported distribution static compensator for power quality enhancement in three-phase four-wire distribution system, Int. J. Hydrogen Energy 39 (2014) 19051-19066.

[16] J.S.R Jang, ANFIS adaptive network based fuzzy inference system, IEEE Trans. Syst. Man Cybern. 23 (1993) 665-684.

[17] S. Lalouni, D. Rekioua, T. Rekiou, E. Matagne, Fuzzy logic control of stand-alone photovoltaic system with battery storage, J. Power Sources 193 (2009) 899–907.

[18] N. Chettibi, Adel Mellit, FPGA-based real time simulation and control of grid-connected photovoltaic systems, Simul. Modell. Pract. 43 (2014) 34-53.

[19] V. Kamatchi Kannan, N. Rengarajan, Photovoltaic based distribution static compensator for power quality improvement, Int. J. Electr Power Energy Syst. 42 (2012) 685-692.

[20] B. Singh, P. Jayaprakash, D.P. Kothari, A T-Connected Transformer and Three-leg VSC Based DSTATCOM for Power Quality Improvement, IEEE Trans. Power Electron. 23 (2008) 2710-2718.

[21] P. Kumar, N. Kumar, A.K Akella, A simulation based case study for control of DSTATCOM, ISA Trans. 53 (2014) 767–775.

[22] P. Jayaprakash, B. Singh, D.P. Kothari, Digital Signal Processor Implementation of Isolated Reduced-rating Voltage Source Converter Using a Zig-zag Transformer for Three-phase Four-wire Distribution Static Compensator, Electr Power Compon Syst. 39 (2011) 15-30.

[23] Ishaque, Kashif, Zainal Salam, Hamed Taheri, Modeling and simulation of photovoltaic (PV) system during partial shading based on a two-diode model, Simul. Modell. Pract. 19 (2011) 1613-1626.

[24] N. Pandiarajan, R. Muthu, Mathematical Modeling of Photovoltaic Module with Simulink, in: Proc of International Conference on Electrical Energy System, 2011.

[25] A. Mäki, V. Valkealahti, Differentiation of multiple maximum power points of partially shaded photovoltaic power generators, Renewable Energy 71 (2014) 89-99.

[26] W. Jiang, Y.F. Zhou, J.N. Chen, Modeling and simulation of boost converter in CCM and DCM, in: Proc of IEEE Conference on Power Electronics and Intelligent Transportation System (PEITS), 2009.

[27] H. Mokhtari, S.B. Dewan, M.R. Iravani, Analysis of a Static Transfer Switch With Respect to Transfer Time, IEEE Trans. Power Delivery 17 (2002) 190-199.

[28] M.N. Moschakis, N.D. Hatziargyriou, A detailed model for a thyristor-based static transfer switch, IEEE Trans. Power Delivery 18 (2003) 1442-1449.

[29] S. Jazebi, S.H. Hosseinian, B. Vahidi, DSTATCOM allocation in distribution networks considering reconfiguration using differential evolution algorithm, Energy Convers. Manage. 52 (2011) 2777–2783.

[30] B. Singh, S.K. Dube, S.R. Arya, An improved control algorithm of DSTATCOM for power quality improvement, Int J Electr Power Energy Syst. 64 (2015) 493–504.

[31] W.J Xiao, Z.J. Xin, C.Y. Guang, T.Y. Heng, Nonlinear modeling of a SOFC stack based on ANFIS identification, Simul. Modell. Pract. 16 (2008) 399-409.

[32] T. Zaveri, B. Bhalja, N. Zaveri, Comparison of control strategies for DSTATCOM in three-phase, four-wire distribution system for power quality improvement under various source voltage and load conditions, Int. J. Electr Power Energy Syst. 43 (2012) 582-594.